Nonlocal spin transport in single-walled carbon nanotube networks

Hyunsoo Yang,[1,*] Mikhail E. Itkis,[2] Rai Moriya,[3] Charles Rettner,[3] Jae-Seung Jeong,[4] Daniel S. Pickard,[1] Robert C. Haddon,[2] and Stuart S. P. Parkin[3]

[1]*Department of Electrical and Computer Engineering, National University of Singapore, 4 Engineering Drive 3, 117576 Singapore*

[2]*Center for Nanoscale Science and Engineering, Departments of Physics and Astronomy, Chemistry and Chemical and Environmental Engineering, University of California, Riverside, California 92521, USA*

[3]*IBM Almaden Research Center, 650 Harry Road, San Jose, California 95120, USA*

[4]*School of Physics, Korea Institute for Advanced Study, Seoul 130-722, Korea*

(Received 3 September 2011; revised manuscript received 19 December 2011; published 13 February 2012)

Spin transport in carbon-based materials has stimulated much interest due to their ballistic conductance and a long phase coherence length. While much research has been conducted on individual carbon nanotubes, current growth and placement techniques are incompatible with large-scale fabrication. Here, we report on nonlocal spin injection and detection in single-walled carbon nanotube networks. We observe spin transport over a distance of 1 μm and extract a spin diffusion length of 1.6–2.4 μm with an injected spin polarization from CoFe into nanotube network of 18%–41%. Our observations demonstrate that spin transport is possible in carbon nanotube networks due to the formation of natural tunnel barriers between nanotubes and metallic contacts.

DOI: 10.1103/PhysRevB.85.052401 PACS number(s): 85.75.−d, 72.25.Dc

Spin-based devices benefit greatly from long spin coherence times and distances. Among the spin transport media studied to date, semiconductors have the advantage of longer spin relaxation times compared to metals, but they also have smaller carrier velocities. In principle, carbon nanotubes (CNTs) are a promising alternative media for the transport of spin information, because they have weak hyperfine interactions, long spin relaxation times, and large spin travel velocities. Local and nonlocal magnetoresistances (MRs) have been reported in single CNT nanowires.[1–11] However, the self-assembly-style growth of CNTs is not well suited to top-down device fabrication for mass production, yielding only a few working devices per wafer. Here, we show that single-walled carbon nanotube (SWNT) networks, where the nanotubes are in the form of densely packed thin films, are appealing candidates for spintronic applications. We show that the resistance of a ferromagnetically contacted nanotube network switches hysteretically as a function of the applied magnetic field in a nonlocal geometry, which is due neither to the anisotropic MR nor to the anomalous Hall effect in the ferromagnetic leads.

For this work, we utilized highly purified, electric arc discharge–produced SWNTs of average diameter: 1.55 ± 0.1 nm.[12,13] SWNT thin films were prepared by vacuum filtration of a SWNT dispersion using an alumina filtration membrane disk (47 mm diameter, 0.02 μm pore size, and 34 mm working diameter) following procedures in the literature.[14,15] The thickness of the SWNT films was controlled by the amount of the SWNT material utilized for the vacuum filtration, taking into account the working area of the filtration membrane; the final thickness calibration was obtained using a Dektak profilometer on thicker (>200 nm) SWNT films. All data in this Brief Report were taken on films prepared from a dispersion of 0.060 mg of SWNT material in 100 mL of solvent with a resulting thickness of the SWNT film of 50 nm, which corresponds to a SWNT film density of 1.2 g/cm^3.[16] The SWNT film was separated from the alumina membrane by dipping into a 0.05N NaOH solution, followed by the transfer of the free-floating SWNT film in deionized (DI) water. The SWNT film was then placed at the designated position on the patterned Si wafer by using a DI waterdrop transfer method in which the DI water was carefully removed using capillary forces. The procedure was completed by rinsing the wafer with the SWNT film with acetone and isopropyl alcohol and drying at 150 °C in a vacuum of 10^{-6} torr for two hours. A scanning electron microscopy (SEM) image of a typical CNT network is shown in Fig. 1(a). There is no preferential orientation of CNTs because the vacuum filtration procedure of the film formation leads to random placement of SWNTs.[17,18] The typical resistivity is ∼0.002 Ω ·cm at room temperature, but it increases by 10–20 times from 300 to 4.2 K.

Figure 1(b) shows a scanning helium ion microscope (HIM) image of a device with a CNT network channel and four magnetic electrodes (F_1–F_4). A rectangular spin transport channel in Fig. 1(b) is defined by standard e-beam lithography followed by an oxygen plasma treatment. The contact pads consist of Cr (10 nm)/Au (90 nm), and the four ferromagnetic leads of $Co_{70}Fe_{30}$ (2 nm)/$Co_{49}Fe_{21}B_{30}$ (10 nm)/Ta (4 nm)/TaN (4 nm) on top of the CNT network channel are deposited by magnetron sputtering. As shown in Fig. 1(c), one of the ferromagnetic electrodes, F_2, is designed to have a smaller width than the other three electrodes (i.e., 200 nm compared to 300 nm) so that its magnetization switches at a higher magnetic field. Because of the nature of the nanofabrication process, each ferromagnetic electrode may have slightly different switching fields—even though they are designed to have the same width. Because the reported spin coherence length of CNTs is no more than 1 μm, the channel length L in this study is varied from 100 to 800 nm.[1,4] Among 24 fabricated devices with different channel lengths, 12 devices were tested in the nonlocal geometry and 9 devices showed nonlocal switching hysteresis. Because the nonlocal measurement geometry in Fig. 1(c) completely separates the charge and spin current paths, any spurious MR effect is eliminated.[6,7]

The junction resistance was investigated by using two- and four-terminal local direct current measurements, as shown in Fig. 1(d) and 1(e), respectively. The magnetic field was applied along the easy axis of the ferromagnetic electrodes,

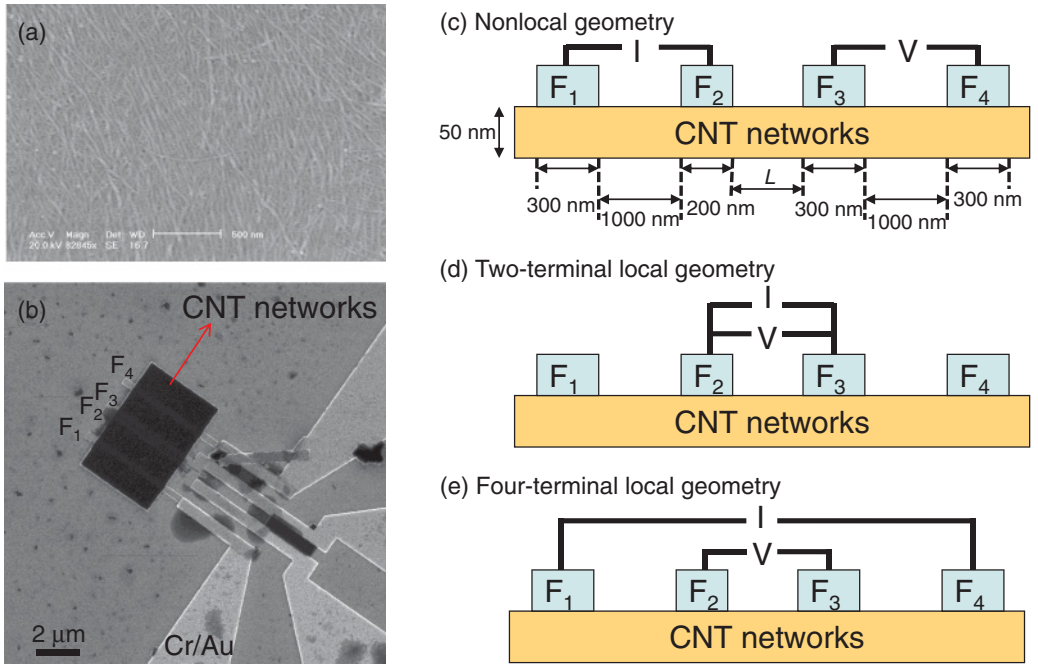

FIG. 1. (Color online) (a) SEM image of a SWNT network. The scale bar is 500 nm. (b) The scanning HIM image of the fabricated device with four ferromagnetic electrodes (F_1–F_4) and Cr/Au contact pads. (c) The nonlocal spin valve measurement geometry. (d) Geometry of a two-terminal local measurement. (e) The four-terminal local geometry.

which is perpendicular to the current direction in the CNT network channel. At room temperature, the junctions show ohmic characteristics, as shown in Fig. 2(a) and 2(c), whereas the current–voltage (I-V) curves show nonlinear properties at 6 K, as illustrated in Fig. 2(b) and 2(c). As fitted in Fig. 2(b), the current is found to vary according to a power law of the form $I(V) \propto V^{\alpha}$, with $\alpha \approx 2.56$ (eV $<$ 10 mV) and $\alpha \approx 1.30$ (eV $>$ 10 mV) at 6 K, indicating the tunneling behavior.[19,20] Strong repulsive interactions of carriers and the Coulomb blockade effect are responsible for the nonlinear I-V characteristics, which have been reported in CNT devices at low temperatures.[3,4,19] The channel resistance does not scale well with the channel length, as shown in Fig. 2(d), because the contact resistance dominates the total resistance, as can be estimated from the difference between the two- and the four-terminal resistance values.[5,21]

The pure spin current signal can be probed within the nonlocal measurement geometry, which excludes charge current contributions such as those from anisotropic MR, the magneto-Coulomb effect, and the anomalous Hall effect in the ferromagnetic leads. If there is the magneto-Coulomb effect, the junction conductance oscillates or linearly scales with the magnetic field.[22] However, our data do not show such behavior, as explained later. The nonlocal resistance using standard lock-in techniques measured at zero bias is defined as $R = V/I$, as shown in Fig. 1(c). The injection current is $\sim$0.5 μA root-mean-square at a frequency of 41.7 Hz, and constant baseline resistance is subtracted to get spin nonlocal resistance R_S. The measurements were performed at 0.25 K to overcome the conductance mismatch between the channel and the spin injectors by the natural tunnel barrier formed at low temperatures. As can be seen in Fig. 3(a)–3(e), there is a clear hysteresis effect associated with different magnetic configurations due to the switching of four ferromagnetic electrodes. The different magnetization alignments of the CoFe electrodes are indicated by the vertical arrows in Fig. 3. Starting from 0.5 T, all ferromagnetic electrodes are aligned in one direction. As the magnetic field is swept from positive to negative values, the lowest resistance state is achieved when F_1, F_3, and F_4 flip their magnetization directions, e.g., around -0.1 T in Fig. 3(a). In this configuration, the injectors (F_1 and F_2) are antiparallel and the detectors (F_3 and F_4) probe the spatial dependence of the spin-down chemical potentials, resulting in negative nonlocal resistance. As the field is further swept to greater negative values, the magnetizations become parallel again but points in the opposite direction. Ramping up the field to positive values causes the spin signal to increase above the background level at 0.086 T when F_1 and F_4 reverse. In this magnetization alignment, the detection voltage probes opposite spin directions, with both injectors and detectors being antiparallel, resulting in positive nonlocal resistance. When F_3 flips, the detectors probe a negative nonlocal signal; finally, the magnetization is aligned in one direction when F_2 flips.

Some samples show an asymmetric loop with respect to the magnetic field, as in Fig. 3(b). Such loop shifts toward a negative field can be explained by exchange biasing due to the formation of antiferromagnetic oxides such as CoO and FeO_x. Such antiferromagnetic layers below their respective Neel temperatures give rise to a unidirectional anisotropy of the ferromagnetic electrodes and induce an asymmetric MR signal with the magnetic field, as reported previously for multiwalled CNTs, multilayer graphene, and magnetic tunnel junctions.[3,23,24] When there is a strong exchange bias, we only observe a minor loop in which one of the electrodes (F_2) is pinned and does not change its magnetization direction, as shown in Fig. 3(c)–3(e).[25]

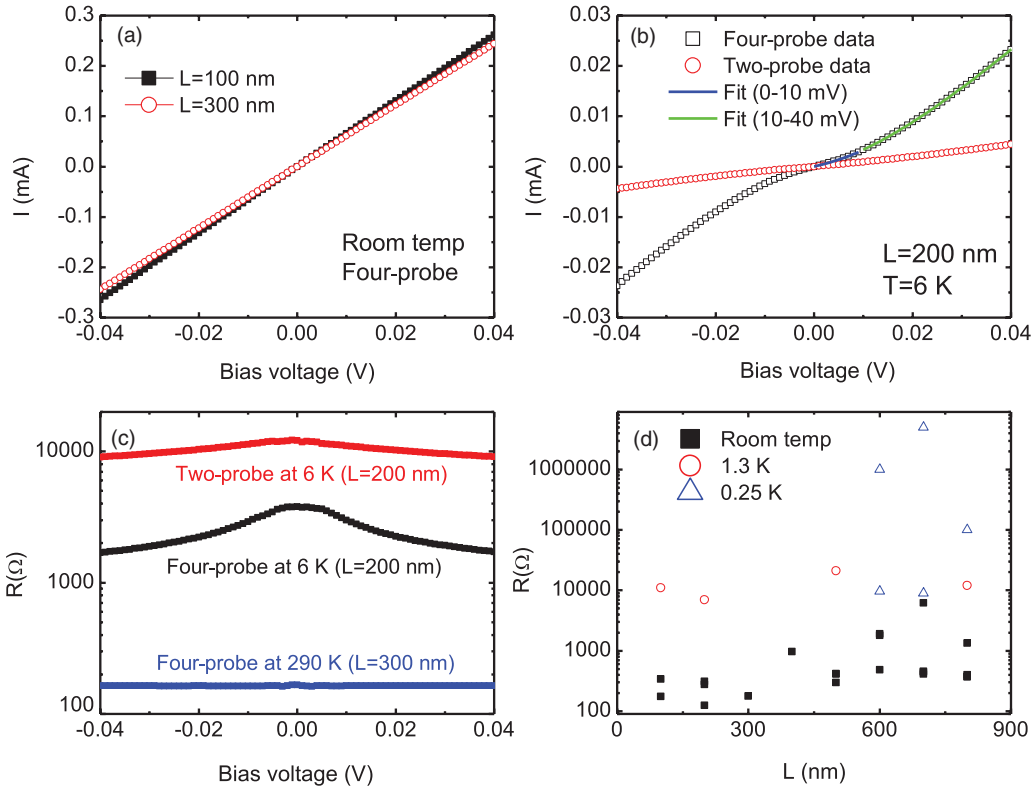

FIG. 2. (Color online) (a) I-V characteristics of devices with different channel lengths at room temperature using a four-probe technique. (b) Comparison of I-V data using two- and four-probe techniques from a device with $L = 200$ nm at 6 K. The solid lines are fits. (c) Resistance versus bias voltage. (d) Resistance versus length at various temperatures.

The staircaselike behavior in the nonlocal switching signal of Fig. 3(a) is attributed to the subsequent sequential switching of the ferromagnetic electrodes due to the formation of ripple domains, which typically is found in thin film materials that have a high saturation magnetization, such as CoFe, used as in our experiments.[8] Because the ferromagnetic electrodes consist of many small magnetic grains and different grains are connected to different individual nanotubes, domain switching at different values of the magnetic field contributes to the multistep signal in Fig. 3(a).[3] However, multiple nanotubes involved in transport can produce gradual switching by averaging the various switching fields, as seen in Fig. 3(b). In an ideal case, the background nonlocal resistance should be zero because there is no charge current flow. However, there are two types of groups, depending on the value of the baseline resistance: one with a large baseline resistance of several kilo-ohms in Fig. 3(a)–3(c) and the other with a relatively small baseline resistance of ∼300 Ω in Fig. 3(d) and 3(e). Finite baseline resistance can be attributed to the finite input impedance if the measurement unit works as a current sink and ballistic carrier motion in the channel.[6,26] Another report has pointed out that interface inhomogeneity can result in finite baseline resistance, which is plausible in our SWNT films.[27] The interplay of Peltier and Seebeck effects on nonlocal baseline resistance can be ruled out in our samples due to a high resistive channel and a low excitation current.[28]

For tunneling contacts using the general theory of nonlocal measurements, the difference in the magnitude of the nonlocal spin signals for the parallel and antiparallel states of the central two electrodes is given by $\Delta R_s = (P^2\rho\lambda/A)e^{-L/\lambda}$, labeled in Fig. 3(a), where P is the injected spin polarization, ρ is the resistivity of the CNT channel, λ is the spin diffusion length, A is the cross-sectional area of the channel, and L is the channel length.[29–31] The dependence of nonlocal MR ($\Delta R_s/R$) versus length is plotted in Fig. 3(f) on a log scale, where R is $\rho L/A$. The solid lines are fitted using the preceding equation, and we obtain values of $\lambda = 1.61$ μm with $P = 0.18$ for the large baseline group (open circles) and $\lambda = 2.45$ μm with $P = 0.41$ for the small baseline group (solid squares). Similar values of the spin diffusion length of 1.4 μm and the spin polarization of 0.2–0.25 have been reported in experiments using a single CNT.[4,6,7] There is a reduction in the injected spin polarization at the interface due to spin flip scattering compared to the spin polarization of 0.55 expected for CoFe.[29,32] The spin resistance mismatch between the channel and the spin injector is overcome by the nonlinear tunneling characteristics between CNTs and CoFe at low temperatures, leading to spin valve voltages V_s in the range 50–70 μV in Fig. 3. An upper bound of the spin relaxation time τ_{sf} can be estimated to be 32.4–75 ps from the relationship of $\lambda = \sqrt{v\tau_{sf}l}$, where the mean electron velocity v in the CNTs is 0.8×10^6 m/s and a CNT mean free path l is 0.1 μm.[20]

Lastly, we discuss the origin of spin relaxation in our measurements. In carbon-based materials, the hyperfine interaction is suppressed due to the absence of nuclear spins in ^{12}C. Thus, effective spin-orbit coupling (SOC) for conducting carriers is mainly responsible for spin relaxation, which is the case for our SWNT film devices. Recently, it was suggested that lattice

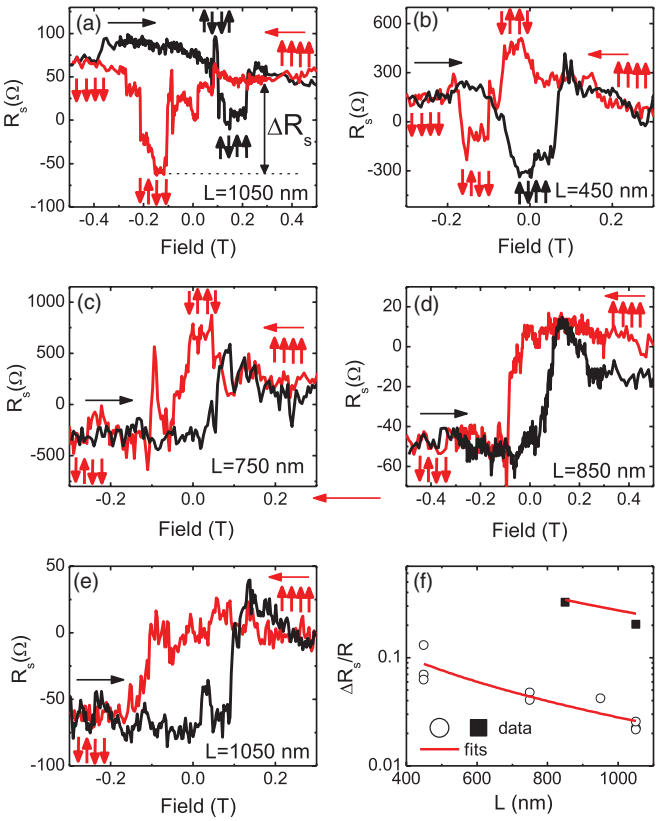

FIG. 3. (Color online) The nonlocal spin signals with various injector and detector spacing lengths measured at 0.25 K. Constant baseline resistance of ∼5–9 k Ω and ∼300 Ω is subtracted in (a)–(c) and (d) and (e), respectively. The spacing is between the central injector and the central detector electrodes. (f) The dependence of nonlocal MR on the spacing. The solid lines are fits.

distortion from sp^2 to sp^3 induced by adatoms chemisorbed on the graphene surface gives rise to the enhancement of local SOC on the order of 10 meV.[33] This adatom-induced SOC is considered an origin of the short spin relaxation time on the order of 0.1 ns in graphene,[34] which could also be an origin of the short spin relaxation time in our SWNT films if it is realizable on the SWNT surface. However, previous theoretical works have revealed that SWNTs are rather inert, so adatoms are more apt to physisorb onto the SWNT surface than to chemisorb.[35,36] Hence, the adatoms on the SWNT surface are least likely to induce SOC. Unlike with graphenes, the cylindrical curvature of SWNTs affects energy dispersion significantly. Combined with atomic SOC, the curvature induces effective SOC on the order of 0.1 meV that was measured experimentally in an ultraclean SWNT quantum dot.[37,38] The strength of curvature-induced SOC depends on the chirality of SWNTs, and the direction of its spin-orbit field is along the SWNT axis.[39,40] As a result, both strength and direction of curvature-induced SOC in our SWNT films consisting of randomly oriented CNTs are spatially random with nanoscale variation [Fig. 1(a)]. In addition, SOC maximum strength can be enhanced to nearly 1 meV for our CNTs with a diameter of 1.55 nm. Therefore, we believe that curvature-induced SOC is a primary source of spin relaxation in SWNT films.

Spin relaxation in SWNT films has not yet been addressed theoretically, but several spin relaxation mechanisms arising from curvature-induced SOC in a SWNT[41–43] and a corrugated graphene[44] have been proposed, which could be useful in analyzing our measurements. For itinerant electrons in a SWNT, curvature-induced SOC can generate fluctuating spin precession, yielding spin relaxation at room temperature that suppresses as temperature decreases.[43] Also, deformation potential[41] and bending-mode phonons[42] in SWNT quantum dots can cause spin relaxation. The estimated spin relaxation times are at least on the order of 1 μs at 0.1 K for SOC on the order of 0.1 meV, which could become at least 10 ns for SOC on the order of 1 meV because spin relaxation rate is proportional to the square of SOC strength. In a corrugated graphene,[44] curvature-induced SOC on the order of 0.01 meV can cause spin relaxation, and its estimated spin relaxation time is ∼100 ns. In this mechanism, the spin relaxation time could be ∼10 ps for SOC on the order of 1 meV, which might imply the importance of random SOC for spin relaxation in our measurement. To estimate a reliable spin relaxation time in SWNT films, we must consider not only random curvature-induced SOC but also intertube transmission of charge carriers in the presence of SOC.

In conclusion, we have succeeded in detecting spin transport in a SWNT film over a distance of 1 μm between CoFe contacts in a CNT network using a nonlocal probe configuration to eliminate spurious MR effects. The measured nonlocal signal (ΔR_s) from a CNT film is comparable to the largest value of 130 Ω observed in graphene.[45] The estimated spin diffusion length in this film at 0.25 K is 1.61–2.45 μm, and the injected spin polarization from CoFe into the nanotube network is found to be 18%–41%. Our observations open the possibility of fabricating many CNT-based spintronic devices in a single wafer using a conventional top-down approach by taking advantage of the long spin diffusion length and the high spin injection efficiency without the need for any artificial tunnel barrier in CNTs. Further experimental works, such as the demonstration of the Hanle effect, and room temperature operation using a tunnel barrier and an aligned nanotube film will make the proposed nanotube networks a promising building block for spin transport devices.

This work is partially supported by the Singapore National Research Foundation under Competitive Research Programme Award No. NRF-CRP 4-2008-06 and the Singapore Ministry of Education under Academic Research Fund Tier 2 (MOE2008-T2-1-105) and Award No. R-263-000-504-133, and by the US Defense Microelectronics Activity (DMEA) under agreement number H94003-10-2-1004.

*eleyang@nus.edu.sg

[1]K. Tsukagoshi, B. W. Alphenaar, and H. Ago, Nature **401**, 572 (1999).

[2]L. E. Hueso, J. M. Pruneda, V. Ferrari, G. Burnell, J. P. Valdes-Herrera, B. D. Simons, P. B. Littlewood, E. Artacho, A. Fert, and N. D. Mathur, Nature **445**, 410 (2007).

[3]B. Zhao, I. Monch, H. Vinzelberg, T. Muhl, and C. M. Schneider, Appl. Phys. Lett. **80**, 3144 (2002).
[4]J.-R. Kim, H. M. So, J.-J. Kim, and J. Kim, Phys. Rev. B **66**, 233401 (2002).
[5]A. Jensen, J. R. Hauptmann, J. Nygård, and P. E. Lindelof, Phys. Rev. B **72**, 035419 (2005).
[6]G. Gunnarsson, J. Trbovic, and C. Schönenberger, Phys. Rev. B **77**, 201405 (2008).
[7]N. Tombros, S. J. van der Molen, and B. J. van Wees, Phys. Rev. B **73**, 233403 (2006).
[8]D. Preusche, S. Schmidmeier, E. Pallecchi, C. Dietrich, A. K. Huttel, J. Zweck, and C. Strunk, J. Appl. Phys. **106**, 084314 (2009).
[9]S. Sahoo, T. Kontos, J. Furer, C. Hoffmann, M. Graber, A. Cottet, and C. Schonenberger, Nat. Phys. **1**, 99 (2005).
[10]H. Aurich, A. Baumgartner, F. Freitag, A. Eichler, J. Trbovic, and C. Schönenberger, Appl. Phys. Lett. **97**, 153116 (2010).
[11]C. Feuillet-Palma, T. Delattre, P. Morfin, J. M. Berroir, G. Fève, D. C. Glattli, B. Plaçais, A. Cottet, and T. Kontos, Phys. Rev. B **81**, 115414 (2010).
[12]M. E. Itkis, D. Perea, S. Niyogi, J. Love, J. Tang, A. Yu, C. Kang, R. Jung, and R. C. Haddon, J. Phys. Chem. B **108**, 12770 (2004).
[13]A. Yu, E. Bekyarova, M. E. Itkis, D. Fakhrutdinov, R. Webster, and R. C. Haddon, J. Am. Chem. Soc. **128**, 9902 (2006).
[14]Z. Wu, Z. Chen, X. Du, J. M. Logan, J. Sippel, M. Nikolou, K. Kamaras, J. R. Reynolds, D. B. Tanner, A. F. Hebard, and A. G. Rinzler, Science **305**, 1273 (2004).
[15]M. E. Itkis, F. Borondics, A. Yu, and R. C. Haddon, Science **312**, 413 (2006).
[16]F. Wang, M. E. Itkis, and R. C. Haddon, Nano Lett. **10**, 937 (2010).
[17]M. E. Itkis, F. Borondics, A. Yu, and R. C. Haddon, Nano Lett. **7**, 900 (2007).
[18]L. Hu, D. S. Hecht, and G. Grüner, Nano Lett. **4**, 2513 (2004).
[19]L. E. Hueso, G. Burnell, J. L. Prieto, L. Granja, C. Bell, D. J. Kang, M. Chhowalla, S. N. Cha, J. E. Jang, G. A. J. Amaratunga, and N. D. Mathur, Appl. Phys. Lett. **88**, 083120 (2006).
[20]A. Bachtold, M. de Jonge, K. Grove-Rasmussen, P. L. McEuen, M. Buitelaar, and C. Schönenberger, Phys. Rev. Lett. **87**, 166801 (2001).
[21]A. F. Morpurgo, J. Kong, C. M. Marcus, and H. Dai, Science **286**, 263 (1999).
[22]H. Shimada, K. Ono, and Y. Ootuka, J. Appl. Phys. **93**, 8259 (2003).
[23]W. H. Wang, K. Pi, Y. Li, Y. F. Chiang, P. Wei, J. Shi, and R. K. Kawakami, Phys. Rev. B **77**, 020402 (2008).
[24]H. Yang, S.-H. Yang, D.-C. Qi, A. Rusydi, H. Kawai, M. Saeys, T. Leo, D. J. Smith, and S. S. P. Parkin, Phys. Rev. Lett. **106**, 167201 (2011).
[25]R. Thamankar, S. Niyogi, B. Y. Yoo, Y. W. Rheem, N. V. Myung, R. C. Haddon, and R. K. Kawakami, Appl. Phys. Lett. **89**, 033119 (2006).
[26]A. Makarovski, A. Zhukov, J. Liu, and G. Finkelstein, Phys. Rev. B **76**, 161405 (2007).
[27]A. T. McCallum and M. Johnson, Nano Lett. **9**, 2350 (2009).
[28]F. L. Bakker, A. Slachter, J. P. Adam, and B. J. van Wees, Phys. Rev. Lett. **105**, 136601 (2010).
[29]S. Takahashi and S. Maekawa, Phys. Rev. B **67**, 052409 (2003).
[30]F. J. Jedema, H. B. Heersche, A. T. Filip, J. J. A. Baselmans, and B. J. van Wees, Nature **416**, 713 (2002).
[31]M. Johnson and R. H. Silsbee, Phys. Rev. Lett. **55**, 1790 (1985).
[32]H. Yang, S.-H. Yang, C. Kaiser, and S. Parkin, Appl. Phys. Lett. **88**, 182501 (2006).
[33]A. H. Castro Neto and F. Guinea, Phys. Rev. Lett. **103**, 026804 (2009).
[34]C. Ertler, S. Konschuh, M. Gmitra, and J. Fabian, Phys. Rev. B **80**, 041405 (2009).
[35]S.-H. Jhi, S. G. Louie, and M. L. Cohen, Phys. Rev. Lett. **85**, 1710 (2000).
[36]V. A. Margulis and E. E. Muryumin, Phys. Rev. B **75**, 035429 (2007).
[37]F. Kuemmeth, S. Ilani, D. C. Ralph, and P. L. McEuen, Nature **452**, 448 (2008).
[38]T. S. Jespersen, K. Grove-Rasmussen, J. Paaske, K. Muraki, T. Fujisawa, J. Nygard, and K. Flensberg, Nat. Phys. **7**, 348 (2011).
[39]W. Izumida, K. Sato, and R. Saito, J. Phys. Soc. Jpn. **78**, 074707 (2009).
[40]J.-S. Jeong and H.-W. Lee, Phys. Rev. B **80**, 075409 (2009).
[41]D. V. Bulaev, B. Trauzettel, and D. Loss, Phys. Rev. B **77**, 235301 (2008).
[42]M. S. Rudner and E. I. Rashba, Phys. Rev. B **81**, 125426 (2010).
[43]Y. G. Semenov, J. M. Zavada, and K. W. Kim, Phys. Rev. B **82**, 155449 (2010).
[44]J.-S. Jeong, J. Shin, and H.-W. Lee, Phys. Rev. B **84**, 195457 (2011).
[45]W. Han, K. Pi, K. M. McCreary, Y. Li, J. J. I. Wong, A. G. Swartz, and R. K. Kawakami, Phys. Rev. Lett. **105**, 167202 (2010).